applied sciences

MDPI

Article

Comparative Study on Handheld, Modular, and Laboratory Raman Instruments for the Analysis of Colon Tissues and Colorectal Polyps

Alla Synytsya [1,*], Zuzana Kováčová [1], Daniela Janstová [1], Michal Vočka [2], Jaromír Petrtýl [3] and Luboš Petruželka [2]

[1] Department of Analytical Chemistry, University of Chemistry and Technology Prague, Technická 5, 16628 Prague, Czech Republic; kovacovz@vscht.cz (Z.K.); janstovd@vscht.cz (D.J.)
[2] Department of Oncology, First Faculty of Medicine, Charles University in Prague and General University Hospital in Prague, U Nemocnice 2, 12800 Prague, Czech Republic; michal.vocka@vfn.cz (M.V.); lubos.petruzelka@vfn.cz (L.P.)
[3] Fourth Internal Clinic—Gastroenterology and Hepatology, First Faculty of Medicine, Charles University in Prague and General University Hospital in Prague, U Nemocnice 2, 12800 Prague, Czech Republic; jaromir.petrtyl@vfn.cz
* Correspondence: sinical@vscht.cz

Featured Application: Use of portative Raman instruments in clinical investigation of colon tissue samples.

Abstract: Portable Raman spectrometers may offer advantages for clinical medical diagnostics over laboratory instruments by allowing for quick measurements in the field and provision of data suitable for screening analyses. This work evaluates the potential of using available handheld, modular, and laboratory Raman spectrometers for screening normal colon tissues and benign and malignant colon polyps. The Raman spectra of tissue samples and reference biological macromolecules were measured with these instruments and analyzed using curve fitting and multivariate statistics. The spectra of calf thymus DNA measured with portable devices showed suitable signal-to-noise levels and half-widths of the prominent bands. Band positions, resolution, and relative intensities in the Raman spectra of colon tissues and reference compounds varied for the instruments, and the laboratory device demonstrated the best spectral feature. The principal component analysis (PCA) of the spectra obtained with all Raman devices showed well discrimination of normal colon tissue, adenomatous polyp, and adenocarcinoma. Dendrograms of similarity obtained using hierarchy cluster analysis (HCA) for the Raman spectra of all three devices also showed good separation of these samples. The soft independent modeling of class analogy (SIMCA) and support vector machine (SVM) models efficiently classified normal colon tissues and benign/malignant colorectal polyps based on the Raman data from all three devices. Despite its less pronounced spectral characteristics, the handheld Raman spectrometer can be used in early diagnosis of colorectal carcinoma, comparable to the modular and laboratory instruments.

Keywords: portable Raman instruments; early cancer diagnosis; colorectal carcinoma; colon tissues; discrimination analysis

Citation: Synytsya, A.; Kováčová, Z.; Janstová, D.; Vočka, M.; Petrtýl, J.; Petruželka, L. Comparative Study on Handheld, Modular, and Laboratory Raman Instruments for the Analysis of Colon Tissues and Colorectal Polyps. *Appl. Sci.* **2024**, *14*, 791. https://doi.org/10.3390/app14020791

Academic Editors: István Csarnovics and Maria Filomena Botelho

Received: 18 November 2023
Revised: 6 January 2024
Accepted: 9 January 2024
Published: 17 January 2024

1. Introduction

The past decade saw significant progress and the widespread integration of modern technologies into daily life. The development of artificial intelligence and novel smart technologies provides immense relief to society [1]. The main advantage of introducing new technologies is that it is easy and quick to obtain objective results right on the spot, which allows for quick decisions in various life situations. Clinical diagnosis is one of

the areas that require rapid results of screening analyses, especially in the case of severe diseases like colorectal carcinoma [2]. Quickly obtaining a test result and determining a preliminary diagnosis can play a decisive role in saving a human life.

Modern technologies that can be useful in clinical diagnosis include Raman spectroscopy [3]. This is a non-destructive method of molecular spectroscopy based on measuring the energy of inelastic scattering emitted by pre-excited sample molecules [4]. The Raman spectrum provides chemically specific information about the biological and biochemical components in cellular and tissue environments. It helps to identify and reveal anomalies in the composition and structure of biological tissues [5]. Although Raman spectroscopy principles have been known for almost a century, recent advancements in instrumentation and operation have expanded the potential of this method for use in various environments. It also appears to be a promising diagnostic tool using intrinsic markers and, thus, provides biochemical information without the need for additional fluorescent or radioactive labeling [6].

In research and routine laboratory conditions, Raman spectrometers commonly deal with clinical samples obtained from patients and stored, whether modified or unmodified, for ex vivo analysis only. However, the clinical practice needs Raman equipment for both in vivo and ex vivo configurations, and portable tools are preferable for rapid and non-invasive diagnoses [7–9].

The term "laboratory" in the context of Raman spectrometers defines a system where all necessary components are permanently in the laboratory where the measurements occur. On the other hand, "modular" is a portable system where one or more components are located externally and connected to the main body (the spectrometer). Finally, "handheld" refers to a miniature system manipulated by holding it in the hands, with all components in one body [10].

The modular variants of Raman spectrometers are suitable for repeating routine analyses at clinical laboratories, and the fiber optic probes permit us to use them for in vivo examinations. Further minimization led to the development of handheld Raman spectrometers that open up possibilities for measurement in current clinical practice, routine analysis in field conditions, and obtaining results in real time. The handheld systems, unlike their portable modular and laboratory counterparts, are compact autonomous systems in which Raman spectra are often displayed on a handheld unit display, allowing for a more unrestricted approach to performing testing at a lower cost, with ease of transport, and with handling in a variety of environments such as places of ambulatory care. Today, the application area of handheld Raman spectrometers includes forensic science [11], analysis of pharmaceuticals and vaccines [12,13], food authenticity and safety monitoring [14–16], and even known attempts at clinical medical diagnosis [10,17–19].

Colorectal cancer (CRC) is the third most common type of malignancy, after prostate cancer in men and breast cancer in women. It is a frequent disease with a relatively high mortality rate due to its late detection at advanced stages when the treatment options are more aggressive, expensive, and have a poor prognosis [20]. Virtually all cases of CRC arise from adenomatous colorectal polyps, which can transform into carcinoma over time. It is possible to prevent this process by early detection and removal of adenomatous polyps before their malignant transformation. The development of screening methods and the involvement of the non-symptomatic population over fifty years old in the National Colorectal Cancer Screening Program show a positive trend in the decrease in mortality from colorectal cancer [21,22]. Colonoscopy is now considered the "gold standard" diagnostic and treatment tool for detecting and removing neoplasms, biopsy lesions, and asymptomatic colorectal polyps by screening the mucosa of the large intestine. However, a definitive diagnosis of CRC requires the histological examination of biopsy tissue samples. It is one of the slowest steps of the screening examination, taking about 10–14 days. Moreover, it requires complex preparative procedures for tissue samples, and the result depends on the pathologist's experience [23,24]. The biopsy examination using a handheld Raman spectrometer could improve diagnosis and treatment decisions.

This work considers and compares the capabilities of a handheld Raman spectrometer with already proven, higher-category modular and laboratory instruments in terms of its efficacy in a screening assay aimed at the clinical diagnosis of colorectal adenocarcinoma. For this study, we selected representative samples of normal colon tissue and benign and malignant colorectal polyps evaluated through a histological analysis. The expected results will contribute to the development of screening methods and the involvement of new instrumental technologies in the timely detection of early stage cancer disease. With the help of such screening assisted with a handheld Raman device, the attending physician could determine the correct diagnosis directly during the examination of the patient and, thereby, improve the prognosis, use more gentle methods of therapy, and enhance the quality of treatment.

2. Materials and Methods

2.1. Tissue Samples and Reference Compounds

Human colorectal tissues were obtained from patients of the Fourth Internal Clinic—Gastroenterology and Hepatology of the First Faculty of Medicine and the General University Hospital in Prague (Charles University, Prague, Czech Republic) at routine colonoscopic examinations. The samples included control colon tissue cuts without pathological changes, colon polyps of benign tubulovillous adenoma with low-grade dysplastic changes, and colon polyps of invasive adenocarcinoma.

The histological examination of colorectal tissues occurred at the Institute of Pathology of the First Faculty of Medicine and General Teaching Hospital. All patients who agreed to participate in this project signed their informed consent. The Ethics Committee of the First Faculty of Medicine and the General University Hospital in Prague gave the ethical approval (No. 1173/20/S) of this study (No. 45/19, grant AZV 2020VF).

The reference standards of calf thymus DNA, human serum albumin (HSA), rat tail collagen, and sodium hyaluronate from *Streptococcus equi* corresponding to major tissue macromolecules were purchased from Sigma Aldrich (St. Louis, MO, USA). The spectroscopic measurements of these compounds were made under the same conditions as the measurements of the colon tissue samples.

2.2. Instrumental Equipment

Three different Raman instruments were used in this comparative study (Figure 1). These are a handheld Raman spectrometer Ahura FirstDefender (Thermo Fisher Scientific, Waltham, MA, USA), modular portative i-Raman Plus spectrometer (B&W Tek Inc., Newark, DE, USA), and laboratory DXR SmartRaman spectrometer (Thermo Fisher Scientific, Waltham, MA, USA). Basic parameters of these instruments are summarized in Table 1.

Before the Raman measurements, the colorectal tissue samples were washed in 0.9% NaCl and dried with filter paper to remove the wash solution. Then, the samples were placed on a polished stainless-steel microscope slide (25 mm × 75 mm × 0.9 mm) (Elliot Scientific, St Albans, UK) and analyzed through Raman spectroscopy using different Raman spectrometers at 22 °C. The spectra of each sample were recorded at 25–30 independent sites.

2.2.1. Measurement with Handheld Raman Spectrometer

The measurement of reference compounds and tissue samples with a handheld Ahura FirstDefender instrument (λ_{ex} 785 nm) was performed in automatic mode with a spectral resolution of 7–10.5 cm^{-1} for up to 1–3 min. The power of the laser focused on the sample was ~75 mW.

2.2.2. Measurement with Modular Raman Spectrometer

The measurement of reference compounds and tissue samples with a mobile i-Raman Plus spectrometer (λ_{ex} 785 nm) was provided in macroscopic mode using fiber optic probe.

The spectra were recorded in the region of 175–3110 cm^{-1} with spectral resolution of 4.5 cm^{-1}. Each spectrum was generated through the accumulation of 3–10 scans with a laser exposure time of 60–90 s per scan. The laser output power was ~90 mW.

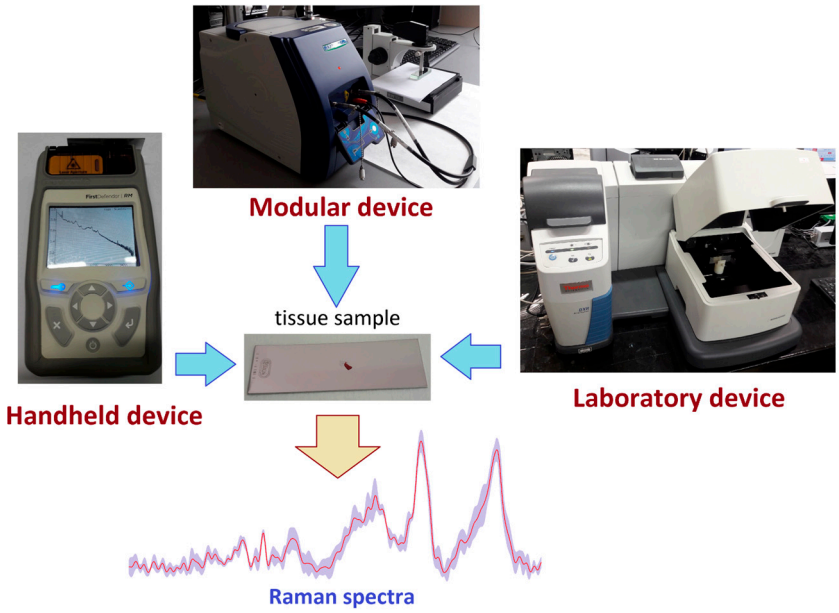

Figure 1. Laboratory and portable Raman instruments used in the measurement of colon tissue samples.

Table 1. Comparison of laboratory, modular, and handheld Raman instruments used in this work.

Characteristics	Types of Raman Instruments		
	Laboratory	Portable	
		Modular	Handheld
Specification	DXR SmartRaman	i-Raman Plus 785H	Ahura FirstDefender
Company	Thermo Fisher Scientific	B&W Tek Inc.	Thermo Fisher Scientific
Address	Waltham, MA, USA	Newark, DE, USA	Waltham, MA, USA
Size (cm)	91 × 63 × 34	17 × 34 × 23.4	19.3 × 10.7 × 4.4
Weight (kg)	>50	3	0.8
Computer	Desktop, serial port	Laptop, USB	Internal software
Excitation wavelength (nm)	780	785	785
Laser outlet power (mW)	90	90 (<300)	75
Detector	CCD	CCD	CCD
Spectral range (cm^{-1})	100–3409	175–3110	250–2875
Spectral resolution (cm^{-1})	2.4–4.4	4.5	7–10.5
Number of scans	3–100	3–10	1
Measuring time (min)	3–100	6–60	1–3

2.2.3. Measurement with Laboratory Raman Spectrometer

The measurement of tissue samples with a DXR SmartRaman Raman spectrometer was performed in macroscopic mode using a sample holder. This instrument is equipped with a DXR 780 nm HP Laser and a diffraction grid comprised of 400 lines per mm. The power of the laser output was ~90 mW. The final spectra were obtained by averaging 3–100 scans, each with an exposure time of 20–60 s. The spectra were measured in a spectral region of 100–3409 cm^{-1} with a resolution of 2.4–4.4 cm^{-1}.

2.3. Processing of Raman Spectra

Raman spectra of the reference compounds and colon tissue samples were exported to Origin 6.0 (Microcal Origin, Northampton, MA, USA) software as the ASCII data files for further processing (FFT filter smoothing by 5 points, manual baseline correction). The mean

spectra and standard deviations were calculated for 25–30 measurements at independent sites of the samples of colon tissue, adenomatous polyp, and colorectal adenocarcinoma.

For all the Raman instruments, the working spectral region of Raman spectra (600–1800 cm^{-1}) of calf thymus DNA was analyzed using the normalized least-squares curve-fitting procedure (PeakFit module of Origin 6.0) using multiple Voigt (Gaussian-Lorentzian mix) curves. The best curve-fitting was specified by the lowest possible χ^2 values. The calculation of the bandwidth at half maximum (BWHM) of ten selected bands in the Raman spectra of calf thymus DNA was obtained from the parameters of the corresponding Voigt components in order to compare the effective spectral resolution between instruments. The signal-to-noise ratio (SNR) for the same bands was calculated by dividing the signal intensity in the raw spectra by the noise level in the operating region of the spectrum. The noise level was defined as twice the standard deviation (SD) of the difference between the original and smoothed spectra [25]. These steps were applied to obtain the noise level near each studied Raman band.

The individual Raman spectra of tissue samples were imported to Unscrambler X 10.5.1 (CAMO Software AS, Oslo, Norway) software for a statistical evaluation, using discrimination analyses, i.e., hierarchy cluster analysis (HCA) and principal component analysis (PCA), for the working spectral region (600–1800 cm^{-1}). This is the region of prominent bands corresponding to stretching and deformation vibrations of the main biological compounds like proteins, nucleic acids, and polysaccharides. Clustering was performed using Ward's method and squared Euclidean distance for 3 clusters. PCA was applied with mean center data for four principal components using singular value decomposition (SVD). The results of the HCA and PCA were represented by dendrograms and component score plots, respectively.

Based on the PCA models generated for each class, i.e., normal colon tissue, adenomatous polyps, and adenocarcinoma, represented by 25–30 measurements in independent regions of the sample, the soft independent modeling of class analogy (SIMCA) algorithm was implemented using Unscrambler X 10.5.1. For each representative sample, training spectroscopic data were collected to represent the spectral particularity of normal colon tissue, adenomatous colorectal polyp, and adenocarcinoma, including their inherent variability caused by the heterogeneity in structure and biochemical composition. For this purpose, PCA was carried out separately for each class of the training sample of 75 spectra (25 independent measurements for each class) in the range of 600–1800 cm^{-1}. The SIMCA model consisted of 7 PCs in each class. After performing PCA on the test data, it was projected into the 7-dimensional data space of each model and assigned to the class with the closest distance. SIMCA results were presented as 3D Cooman's plots of residual distances. Individual Raman spectra in the range of 600–1800 cm^{-1} for all classes of tissue samples and all Raman instruments were also classified using support vector machine (SVM) models. A linear kernel algorithm was selected for the classification task, and the cross-validation process involved ten segments.

3. Results and Discussion

3.1. Specifics of Measurements on Selected Devices

Three Raman instruments, defined as laboratory, modular, and handheld, were used in this work. Each of these selected devices has evident specificity associated with the Raman spectra measurement and related to their design, excitation wavelength, spectral resolution, and other properties. These differences are visible in the example of raw Raman spectra of a calf thymus DNA sample measured with these instruments and adjusted to a unified Raman intensity scale (Figure 2). The handheld Ahura FirstDefender instrument possessed a one-scan Raman spectrum of relatively high noise and low spectral resolution but with several well-resolved signals in the chosen working region of 600–1800 cm^{-1}. The portable i-Raman Plus instrument produces a Raman spectrum with more intense bands and higher signal-to-noise levels corresponding to the spectrum obtained with the Ahura instrument. Finally, the laboratory DXR SmartRaman instrument produces Raman spectra

of the highest resolution and band intensity about noise but needs more measuring time to collect enough scans to obtain a spectrum of good quality. A high-fluorescence background occurred in all cases, and linear mathematics baseline correction was applied to obtain well-representative spectra.

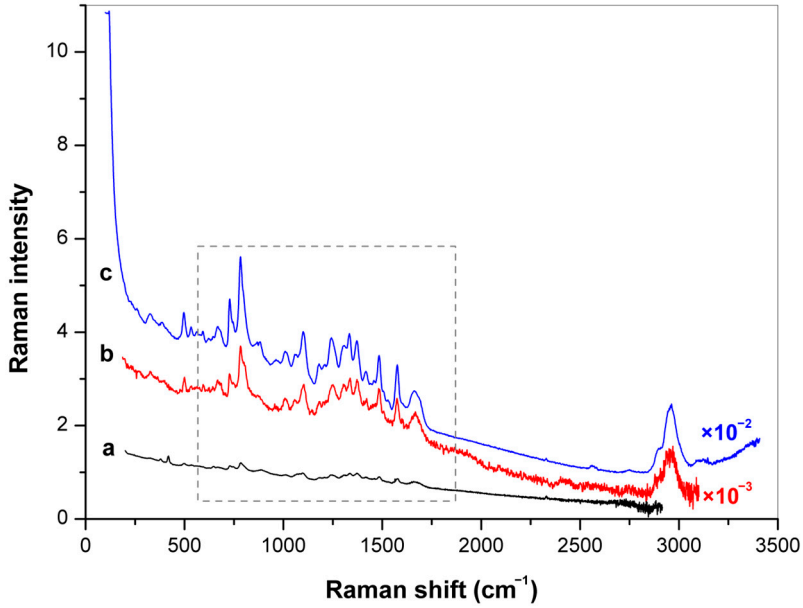

Figure 2. Raw Raman spectra of calf thymus DNA measured using handheld, modular, and laboratory Raman instruments: (a) Ahura FistDefender (75 mW); (b) i-Raman Plus (90 mW; 3 scans; 60 s per scan); (c) DXR SmartRaman (90 mW; 3 scans; 60 s per scan). The dash-line frame indicates the working region ranging from 600 to 1800 cm^{-1}.

A size decrease in Raman spectrometers leads to a simplification of the design and, therefore, to a deterioration in the measurement parameters and the quality of the Raman spectra [26]. It is necessary to compare the spectra obtained on all these instruments to assess the analytical capabilities using the examples of the reference biological macromolecules, colon tissue, and colorectal polyps.

3.2. Spectral Data Comparison between the Instruments

The use of portable devices for recording Raman spectra leads to a higher noise level compared to laboratory instruments due to their smaller size and reduced analysis time, both in the length of one scan and in the number of accumulations [26]. The SNR value is essential for the efficacy of portable Raman devices since the relatively high noise level is their drawback. Using the example of calf thymus DNA Raman spectra, SNR values were obtained for ten selected bands, and they are represented in a histogram (Figure 3a). For all these bands and devices, this value exceeded 9, which confirmed acceptable signal detection. The differences between the devices were significant for all bands, and the DXR SmartRaman showed the highest SNR values (~42–131), followed by i-Raman Plus (~15–30) and Ahura FirstDefender (~9–18). The median SNR value was 70.7 for the DXR SmartRaman, 20.9 for i-Raman Plus, and 12.2 for Ahura; the corresponding mean SNR values were 75.6, 21.2, and 13.1. Relatively low SNR values obtained for portable Raman devices do not limit the use of these instruments for various routine applications where such extremely high sensitivity is not necessary.

The spectral resolution of a portable Raman spectrometer is a crucial measurement parameter to distinguish between several adjacent Raman bands in the spectrum [27]. It is useful, especially in the spectroscopic analysis of animal tissues. Biological macromolecules that constitute cells and tissues, such as proteins, nucleic acids, and polysaccharides, are characterized by complex Raman spectra with many often overlapping bands [5].

Narrower signals in the spectrum enable a better resolution of adjacent bands or shoulders. Otherwise, when the bands become broader, they may appear as shoulders or become indistinguishable. This is especially true for the handheld equipment. Figure S1 represents the multiple-curve fitting analysis of the Raman spectra of calf thymus DNA recorded using the laboratory, modular, and handheld instruments, yielding 18 Voigt components for each spectrum. The histogram in Figure 3b represents bandwidth comparison for selected strong- or moderate-intensity bands detected in the calf thymus DNA spectrum for each instrument. The spectral intervals corresponded to the positions of the Voigt maxima obtained by approximating the peaks, and the bandwidths were also attributes of these components. The BWHM values varied from ~15 to 73 cm^{-1} between bands and devices, and the corresponding average values slightly increased in the order of DXR SmartRaman (33.1 cm^{-1}), i-Raman Plus (35.2 cm^{-1}), and Ahura (35.9 cm^{-1}). Based on the analysis of glycine spectral data, the median BWHM value reported earlier for the Ahura instrument was 14.4 cm^{-1} [28], which is more than twice lower than the value obtained in the present study for the Raman spectrum of DNA. This difference can be explained by the fact that polymeric substances like DNA typically have much wider vibration bands compared to small crystalline molecules, and this broadening of the signals is especially pronounced in amorphous polymers. All instruments of the current study showed more or less similar BWHM values, probably due to the significant overlap of the bands used for calculation. However, it is clear that, at least for the bands at around 1668, 1577, 1373, 1305, 788, and 732–736 cm^{-1}, the laboratory DXR SmartRaman instrument provided spectra with the lowest BWHM compared to the portable systems, for which the handheld device mostly showed higher BWHM values. However, this trend was not observed for the remaining bands at 1100–1336 cm^{-1}.

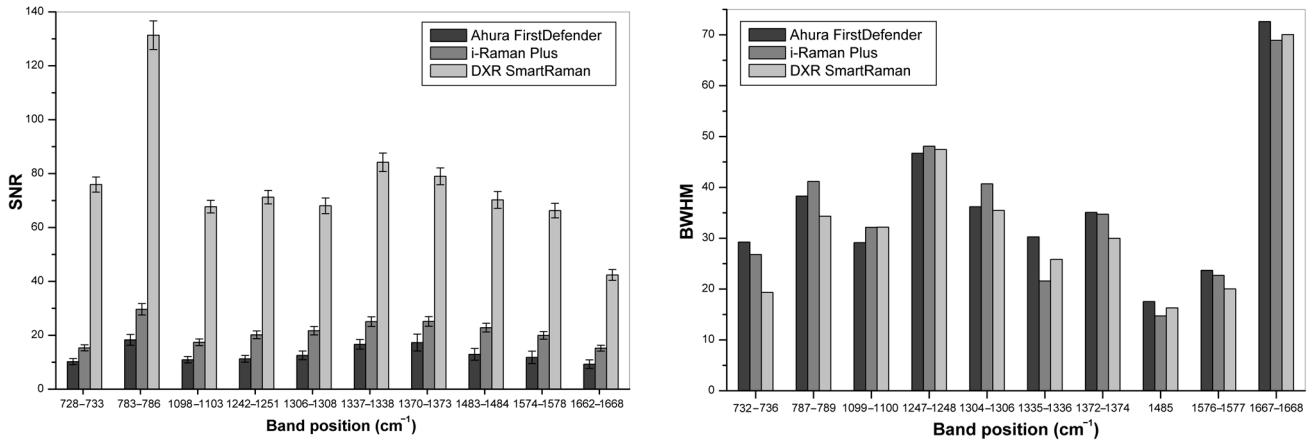

(**a**) (**b**)

Figure 3. Comparison of SNR (**a**) and BWHM (**b**) values for ten chosen Raman bands of calf thymus DNA in the spectra collected with handheld, modular, and laboratory Raman instruments. SNR was calculated by dividing the signal intensity by the noise level in the operating region of the spectrum.

3.3. Raman Spectra of Reference Biological Macromolecules

Figure 4 shows the baseline-corrected and smoothed Raman spectra of model biopolymer compounds, i.e., calf thymus DNA (Figure 4a), human serum albumin (Figure 4b), rat tail collagen (Figure 4c), and bacterial hyaluronic acid (Figure 4d). These reference compounds represent nucleic acids, globular and fibrillar proteins, and polysaccharides glycosaminoglycans, i.e., the classes of biological macromolecules, which constitute colon tissue and participate in many physiological and pathological processes, including carcinogenesis. The Raman spectra of these compounds possess marker bands of macromolecular tissue components, which help interpret the Raman spectra of normal and damaged colon tissues.

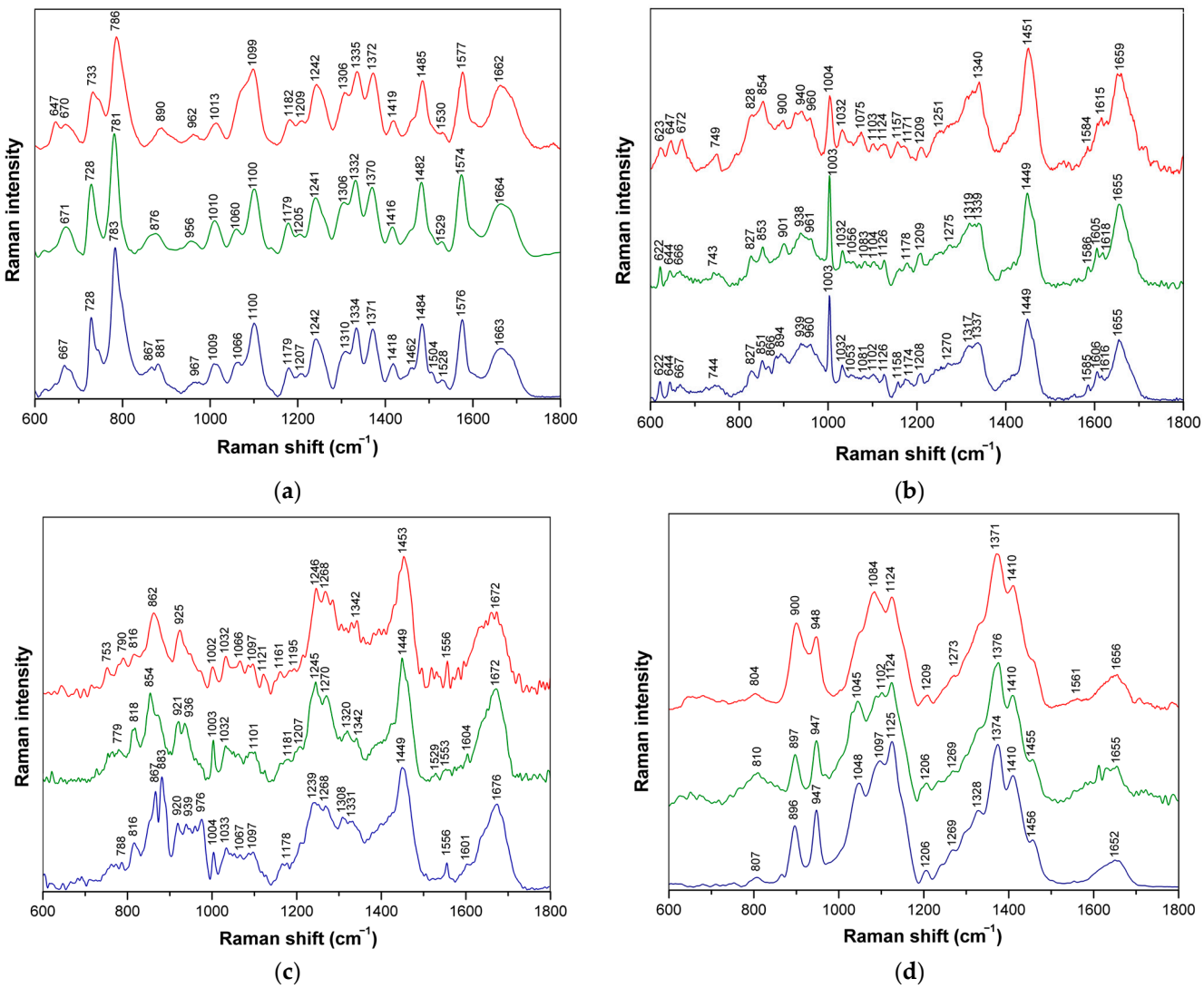

Figure 4. Raman spectra of reference biological macromolecules collected with laboratory (blue), modular (green), and handheld (red) Raman instruments: (**a**) DNA; (**b**) HSA; (**c**) collagen; (**d**) HA.

The spectra measured on the Ahura FirstDefender, i-Raman Plus, and DXR SmartRaman instruments are presented in the working wavenumber range of 600–1800 cm^{-1} and are arranged from top to bottom in rows adjusted to an intensity scale suitable for comparison. The following subsections discuss the wavenumbers of Raman bands obtained for the individual compounds using laboratory and portable instruments and also provide their suggested interpretation based on the literature. Discussion is limited to the most significant Raman bands in the specified spectral region.

3.3.1. Calf Thymus DNA

The spectra of calf thymus DNA measured using different instruments exhibited evident similarity (Figure 4a). Table S1 summarizes the assignments of Raman bands observed for calf thymus DNA. The spectra of calf thymus DNA are dominated by Raman bands of nucleic bases—purines (A, G) and pyrimidines (C, T). There are three main spectral regions in which these bands are localized [29–31]: C=O stretching vibrations (1600–1750 cm^{-1}); in-plane ring deformations of the ring (1000–1600 cm^{-1}); ring breathing and out-of-plane deformations (600–800 cm^{-1}). In addition to these vibrations, the bands of phosphate diester (P) and deoxyribose (dRib) residues also contribute to different regions in the spectrum of DNA.

The positions and relative intensities of the most pronounced peaks are very close, although they vary somewhat within a range of up to 5 cm^{-1}. The band position or intensity deviations observed for portable instruments compared to the DXR SmartRaman could be due to the influence of unresolved nearby bands. The portable instruments, especially Ahura FirstDefender, produced broadened peaks, resulting in a reduced signal resolution and the appearance of shoulders. For example, the spectrum obtained using DXR SmartRaman showed well-resolved weak bands at 1504 and 1462 cm^{-1}. In the case of portable instruments, these bands were observed as shoulders of the peak at 1482–1485 cm^{-1} assigned to the in-plane ring vibrations in purines. The nearest weak band at about 1530 cm^{-1} arose from the C=N stretching vibration in C [29–31]. This band was observed as a shoulder in the spectrum obtained using the Ahura FirstDefender device. DXR SmartRaman and i-Raman Plus devices showed a partially overlapped weak band of the C–O stretching vibration in deoxyribose (dRib) centered at 1066 and 1060 cm^{-1}, respectively [29–31], while the Ahura FirstDefender showed only an unresolved low-frequency shoulder of the strong band at 1099 cm^{-1}, which arose from the symmetric stretching vibration of P. Two intense to medium bands observed at 677, 728, and 783 cm^{-1} and a well-resolved shoulder at 744 cm^{-1} in the spectrum obtained using the DXR SmartRaman were assigned to the ring breathing vibrations in nucleic bases [29–31]. For the Ahura FirstDefender, the corresponding bands were observed at higher frequencies, i.e., 670, 733, and 786 cm^{-1}, due to the adjacent unresolved bands. The shoulder near 744 cm^{-1} was unresolved in the spectra obtained by the portable devices. Among the Raman instruments, these bands are the narrowest for the DXR SmartRaman device, as confirmed by the peak fitting procedure described above.

3.3.2. Human Serum Albumin

The spectra of human serum albumin (HSA) measured using different instruments exhibited evident similarity (Figure 4b). Table S1 summarizes the assignments of Raman bands observed for this protein based on the references [32–34]. With a few exceptions, the position of individual bands in the HSA spectra varies slightly. The evident shifts observed in some peaks are due to different ratios of two or more closely spaced bands depending on the sensitivity and spectral resolution of the instruments. Three strong bands detected in the DXR SmartRaman spectrum at 1655, 1449, 1337, and 1003 cm^{-1} are characteristic of vibrations of amide I, scissoring of methylene groups, C-H deformation, and ring breathing of phenylalanine (Phe), respectively [31]. The i-Raman Plus device showed almost identical wavenumbers for these bands, while for Ahura, the corresponding bands were slightly shifted towards higher frequencies. The spectra clearly show that this band is narrowest for DXR SmartRaman and i-Raman Plus devices and much broader for Ahura FirstDefender. For the laboratory instrument, the tyrosine (Tyr) doublet appeared in the spectrum of HSA as two well-resolved bands at 827 and 851 cm^{-1} [32–34]. In the spectra obtained with both portable devices, this doublet appears unresolved, having the second component resembling a shoulder. Further, in the case of the SmartRaman device, the Trp indole ring vibration band at 866 cm^{-1} is well-resolved [32–34], while in the spectra measured using portable devices, it was observed as a shoulder of the adjacent band at 853–854 cm^{-1}.

3.3.3. Rat Collagen Type I

Fibrillar collagens are connective tissue proteins with a periodic sequence of amino acids and a specific triple helical conformation [35]. They are structurally different from common globular proteins such as HSA and, thus, have distinct Raman spectra with high contributions from the secondary amino acids, Pro and Hyp, and the tertiary amide bonds they form [36–38].

The Raman spectra of collagen type I from rat tail showed a broad band of amide I vibrations with a maximum at 1672–1676 cm^{-1} (Figure 4c, Table S1). The spectrum obtained with Ahura FirstDefender has this band more broadened than those obtained by the other devices. For all instruments, the amide III region has two bands at 1239–1246 and

~1268–1270 cm^{-1} [36–38]. In the DXR SmartRaman spectrum, five bands of C–C stretching and Pro/Hyp ring vibrations observed at 867, 883, 920, 939, and 976 cm^{-1} are well-resolved, but only two or three of them are distinguishable in the spectra recorded with the portable devices. The first two bands are expected to be particularly useful in detecting collagens in Raman spectra of colon tissues [37,38].

3.3.4. Bacterial Sodium Hyaluronate

Hyaluronic acid (HA) is the only non-sulfated glycosaminoglycan (GAG) that plays a prominent role in many physiological and pathological processes in connective tissues [39]. Some microorganisms, such as *Streptococcus*, produce HA as a capsular polysaccharide, whichprotect cells [40]. Sodium hyaluronate (sodium salt of HA) has acetamide (*N*-Ac or N-$COCH_3$) and carboxylate (COO^-) groups originating from *N*-acetyl-*β*-D-glucosamine (GlcNAc) and *β*-D-glucuronic acid (GlcA) units, respectively. The Raman spectra of this polysaccharide measured using laboratory and portable devices (Figure 4d) show similar patterns. Table S1 summarizes band assignments based on the literature [41,42]. The most intense band of the symmetric bending vibration of CH_3 is located at 1374 cm^{-1} for DXR SmartRaman, 1376 cm^{-1} for i-Raman Plus, and 1371 cm^{-1} for Ahura FirstDefender. The spectrum measured using DXR SmartRaman also has three well-resolved bands at 1328, 1410, and 1456 cm^{-1}, attributed mainly to amide III, symmetric stretch of COO^-, and CH_2 and CH_3 scissoring vibrations, respectively [41,42]. In the spectra recorded using portable instruments, some of these bands are present as shoulders. Similarly, the DXR SmartRaman spectrum shows three well-resolved bands of C–O–C, C–O, and C–C stretching and C–OH bending vibrations at 1048, 1097, and 1125 cm^{-1} [41,42]. For Ahura FirstDefender, the former band is non-resolved. Two bands of the DXR SmartRaman spectrum at 896 and 947 cm^{-1} attributed to the C–O–C symmetric stretching vibration of the glycosidic bonds and amide V vibrations, respectively [41,42], are well resolved in all spectra, while in the case of Ahura FirstDefender, the former band was at slightly higher frequencies, i.e., at 900 cm^{-1}.

The specific contribution of these individual bands to the Raman spectrum of sodium hyaluronate, like the spectra of the reference compounds described above, explains the differences in signal overlap determined by the proximity, intensity, and width of adjacent bands, which, in turn, depend on the technical parameters of the measuring equipment. The spectra of reference compounds obtained using different devices adequately illustrate that the laboratory instrument can obtain spectra of higher resolutions than both portable instruments, which is an advantage when analyzing spectroscopic markers of tissue constituents. Although portable devices have technical limitations compared to laboratory instruments, they can still be used to obtain high-quality spectra of biological macromolecules, which enable the identification of these marker compounds in biological tissues.

3.4. Raman Spectra of Colon Tissues and Colorectal Polyps

Figure 5 represents the average Raman spectra (mean ± SD) of normal colon tissue, adenomatous colorectal polyp, and adenocarcinoma samples collected with handheld, modular, and laboratory Raman instruments. Table S2 summarizes the contribution of biological macromolecules in the Raman spectra of normal colon tissue based on the spectra measured for the reference compounds using the DXR SmartRaman instrument.

Positions, widths, and relative intensities of the bands in the spectra of normal colon tissue varied for the Raman instruments used in this work. The tissue bands in the Raman spectrum measured with DXR SmartRaman were mostly well resolved and indicated the main biochemical constituents. By contrast, two portable devices possessed spectra with less-resolved bands. Comparing the modular and handheld devices, it is clear that i-Raman Plus measured spectrum with narrower and more pronounced signals than Ahura FirstDefender. For example, in the spectrum of normal colon tissue obtained with i-Raman Plus, the signals at 1002, 1032, 1125, 1175, 1207, and 1340 cm^{-1} were narrow and well

resolved, while in the spectrum measured with Ahura FirstDefender, the corresponding signals were broader and sometimes appeared as shoulders.

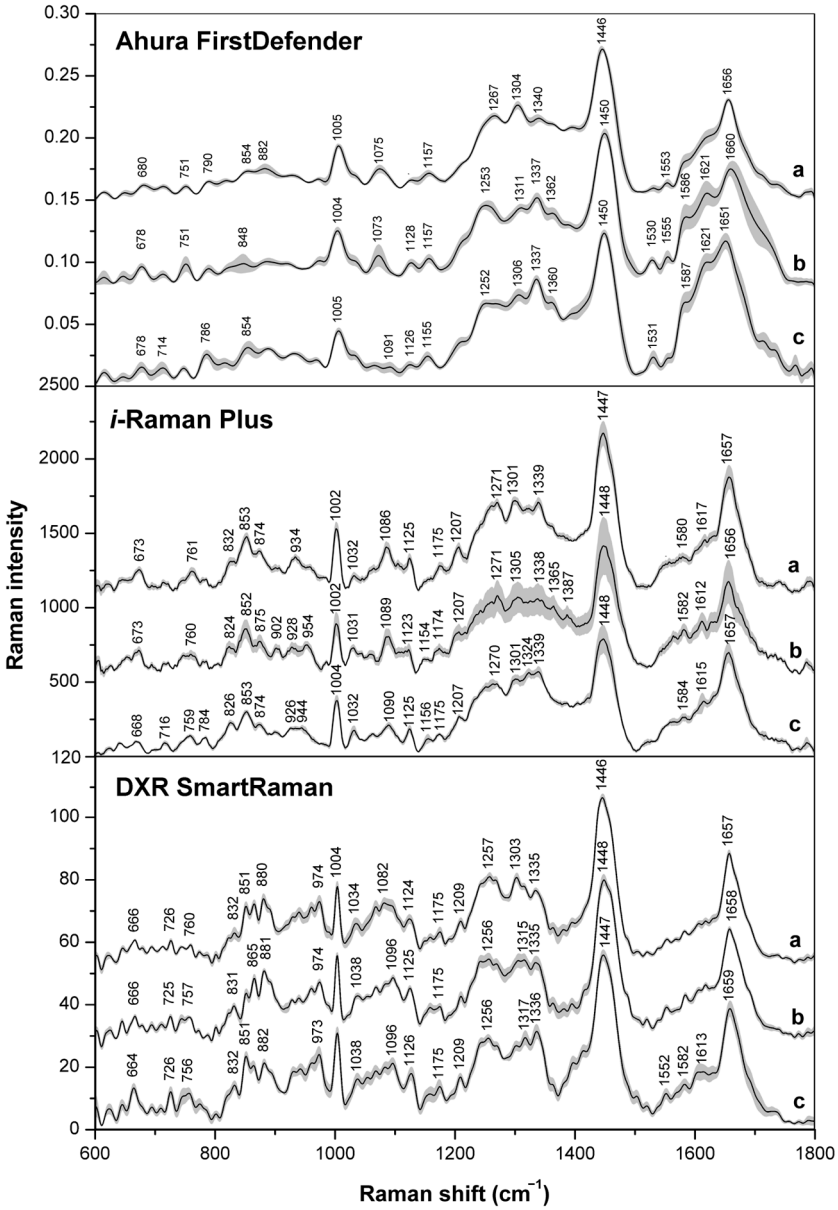

Figure 5. The average Raman spectra of tissue samples collected with handheld (**top**), modular (**middle**), and laboratory (**bottom**) Raman instruments: (a) normal colon tissue; (b) adenomatous colorectal polyp; (c) adenocarcinoma. The standard deviation (SD) intervals are shown as gray space.

The spectra of normal colon tissue have a number of bands characteristic of the main biochemical components: proteins (including collagens), lipids, nucleic acids, and polysaccharides [5,6,43–50]. In addition, many bands include contributions from several biochemical components, making their assignment difficult. Moreover, the contributions of individual components will be far from identical and may differ in their content and location in the tissue sample. The highest contribution to the Raman spectrum of colon tissue comes from protein vibrations. Indeed, the bands observed in the DXR SmartRaman spectrum for normal colon tissue at 1657, 1446, 1335, 1267, 1209, 1124, 1034, 1004, 940, 851, 832, 744, 666, 645, and 622 cm^{-1} were similar to those obtained for HSA (Table S1). These bands are characteristic for vibrations of a protein backbone and amino acid side chains [32,33] and can be used as protein markers. The characteristic bands of nucleic acids

were much less pronounced and may have contributed at 1582, 1335, 1486, 1335, 1303, 1243, 1175, 1095, 880, 786, 726, and 666 cm^{-1} [29–31]. Some of these bands overlapped with the mentioned protein bands, reducing the number of DNA marker bands suitable to follow tissue nucleic acids. Similarly, collagen vibrations contribute to the colon tissue spectrum at 1657, 1636, 1553, 1396, 1381, 1335, 1267, 1245, 1082, 1004, 960, 940, 880, 862, 823, 786, 760, 694, 646, and 622 cm^{-1}, with many of these bands being common to collagens [36–38] and globular proteins [31–34]. Most of the sodium hyaluronate bands do not correspond in position to the tissue peaks, except the bands at 1656, 1267, 1209, and 1124 cm^{-1} [41,42]. More pronounced compounds like proteins contribute to these bands, making them difficult to use for identifying hyaluronate in colon tissue. Hyaluronate macromolecules usually form complexes with other biological molecules or are included in the structure of proteoglycans, so their Raman properties can differ significantly from the properties of pure sodium hyaluronate. Nevertheless, the C–O and C–C stretching bands in the region of 950–1150 cm^{-1} are attributive to tissue polysaccharides like glycogen and GAG [41,42,48], and the intense vibration band of the sulfate groups at 1064–1070 cm^{-1} is suitable for the identification of sulfated GAG [42].

All of these biological macromolecules mentioned above are sensitive to carcinogenesis to varying degrees, which is manifested in more or less pronounced changes in the position and intensity of characteristic bands in the spectra of colorectal adenomatous polyp and adenocarcinoma. However, at least for portable instruments, these spectral differences cannot always be used as pathology markers due to band overlap. In contrast, Raman spectra measured with the DXR SmartRaman instrument can detect even subtle band position and intensity changes, which can be informative when comparing normal and damaged tissues and assessing molecular changes caused by disease progression.

Comparing the Raman spectra of normal colon tissue, adenomatous polyp, and adenocarcinoma, one can note significant differences in the position and intensity of individual bands in some spectral regions. Firstly, the changes occur in the region from 1500 to 1630 cm^{-1}, where the stretching vibrations of aromatic C=C bonds of aromatic amino acids and nucleic bases are located [29–31]. Further, a gradual decline in the band intensity at 1303 cm^{-1} and a simultaneous increase in the band intensity around 1335 cm^{-1} is evident compared to the neighboring band around 1314–1317 cm^{-1}. The first band refers to the twisting vibration of methylene groups primarily in lipids but also in proteins, including collagen, and the second is associated with the C=N stretching vibrations of purines, as well as C_{α}-H bending and triptofan (Trp) vibrations in proteins [5,29,30,47,49]. The changes also occur in the region from 800 to 900 cm^{-1}, where the intensity of the 851 cm^{-1} band is lower in the case of the polyp and, conversely, higher in adenocarcinoma, compared to the neighboring bands around 832, 865, and 880–882 cm^{-1}. The band at 851 cm^{-1} corresponds mainly to the ring breathing vibration of Tyr [32–34], but the C1–H bending of glycogen also contributes here [48]. Finally, one can note the increased intensity of the bands at 664 and 726 cm^{-1} in adenocarcinoma. These two bands arise mainly from the purine ring breathing vibrations [29,30], and the C–S stretching vibration of cysteine (Cys) contributes to the first one [31–33]. Thus, the observed spectral differences between normal colon tissue and benign and malignant polyps, which can be associated with colorectal cancer development, indicate changes in the ratio between such major biochemical tissue components as proteins, nucleic acids, lipids, and polysaccharides [44–47,50]. The above bands, showing significant differences between samples, can be offered as potential markers of carcinogenesis in colon tissue.

3.5. Discrimination of Colon Tissue Samples Based on Raman Data

To properly diagnose colorectal cancer, it is necessary to distinguish between samples originating from normal and abnormal colon tissue, as well as between benign and malignant colorectal polyps. This goal can be achieved by comparing individual characteristic Raman bands of biochemical markers of carcinogenesis or through the discriminatory analysis of Raman spectra using multivariate statistical methods. Previous works have used

various approaches to separate and classify normal and pathological tissue and biofluid samples based on Raman spectra, such as HCA [6,43], PCA [40], partial least squares discriminant analysis (PLS-DA) [51,52], SVM and other machine learning methods [43], PCA in combination with linear discriminant analysis (LDA), SVM, SIMCA [53] and other discriminating parameters like Mahalanobis distance or spectral residuals [45,52,54–57], and convolutional neural networks (CNN) [58–61]. Of particular interest for early cancer diagnosis is the immediate analysis of intracellular Raman spectra using a biomolecular component analysis (BCA) algorithm [62].

In the current work, we used multivariate statistical methods, namely, HCA, PCA, SIMCA, and SVM, to discriminate and classify the individual smoother and baseline corrected Raman spectra of normal colon tissue, adenomatous polyp, and adenocarcinoma samples recorded using handheld, modular, and laboratory Raman instruments at the 25–30 independent sites.

Figure 6 demonstrates the component score plots PC1 versus PC2 (left panels) and dendrograms of similarity (right panels) obtained via HCA using Ward's clustering method and squared Euclidean distances. For all Raman devices, the combination of principal components PC1 and PC2 was found to demonstrate significant differences between the three samples. The best discrimination was observed for spectra measured with Ahura, where well-separated heap clusters of samples were formed. The normal colon tissue sample showed positive PC1 scores, while the corresponding scores of the two abnormal tissue samples were mostly negative. PC2 scores, in turn, separated adenomatous polyp and adenocarcinoma samples into positive and negative regions, respectively. In the case of i-Raman Plus spectra, PC1 partially separated the normal colon tissue sample, which showed negative values for this component, from the abnormal samples, which had mostly positive scores. In turn, PC2 separated the adenocarcinoma sample with negative score values from the remaining two samples. For DXR SmartRaman spectra, PC1 scores of adenocarcinoma fell below −40 and were, thus, separated from the other two samples having higher scores. PC2 separated normal colon tissue and adenomatous polyp, showing negative and mostly positive scores, respectively.

Dendrograms of similarity obtained for the Raman spectra of all three devices showed a good separation of the clusters corresponding to normal colon tissue, adenomatous polyp, and adenocarcinoma. The best discrimination was in the case of Ahura, where all clusters were separated at a distance near 4.5; the corresponding distances were ~6 for i-Raman Plus and ~8.5 for DXR SmartRaman. The Raman spectra measured with both portable instruments showed similar clustering. Firstly, the cluster of normal colon tissue was separated from the abnormal colon tissues. Then, the spectra of adenomatous polyp and adenocarcinoma were split into their clusters. Conversely, for DXR SmartRaman, firstly, the adenocarcinoma was separated from the other two samples, and a discrimination of normal colon tissue and adenomatous polyp occurred at a relatively high distance.

We used PCA-based SIMCA supervised classification to demonstrate Raman spectroscopy's potential in screening colon tissue samples. Among the multivariate data analysis methods, SIMCA can provide a good classification of study groups and high within-class predictability even with small-size datasets [63–65]. The SIMCA model was implemented using Raman data in the working spectral region (600–1800 cm^{-1}) for all three devices based on the three independent PCA models with a significance level of 5%. Three-dimensional Cooman's plots from SIMCA (Figure 7a,c,e) were obtained to visualize the results of the classification analysis. These plots display residual distances for independent measurement points in each sample representing individual classes. As can be seen from the graphs, a clear differentiation of the groups, which referred to the normal colon tissue, adenomatous polyp, and adenocarcinoma, was found for all Raman instruments, and these groups were well classified. For the Ahura FirstDefender and DXR SmartRaman devices (Figure 7a,e), the compact group of normal colon tissue was significantly distant from the more scattered groups of adenomatous polyps and adenocarcinoma, and the latter two groups were closer to each other. However, there was no misclassification of

pathological groups. In contrast, in the case of i-Raman Plus (Figure 7c), all three groups were more scattered and equidistant, but even in this case, there was no overlapping of the groups.

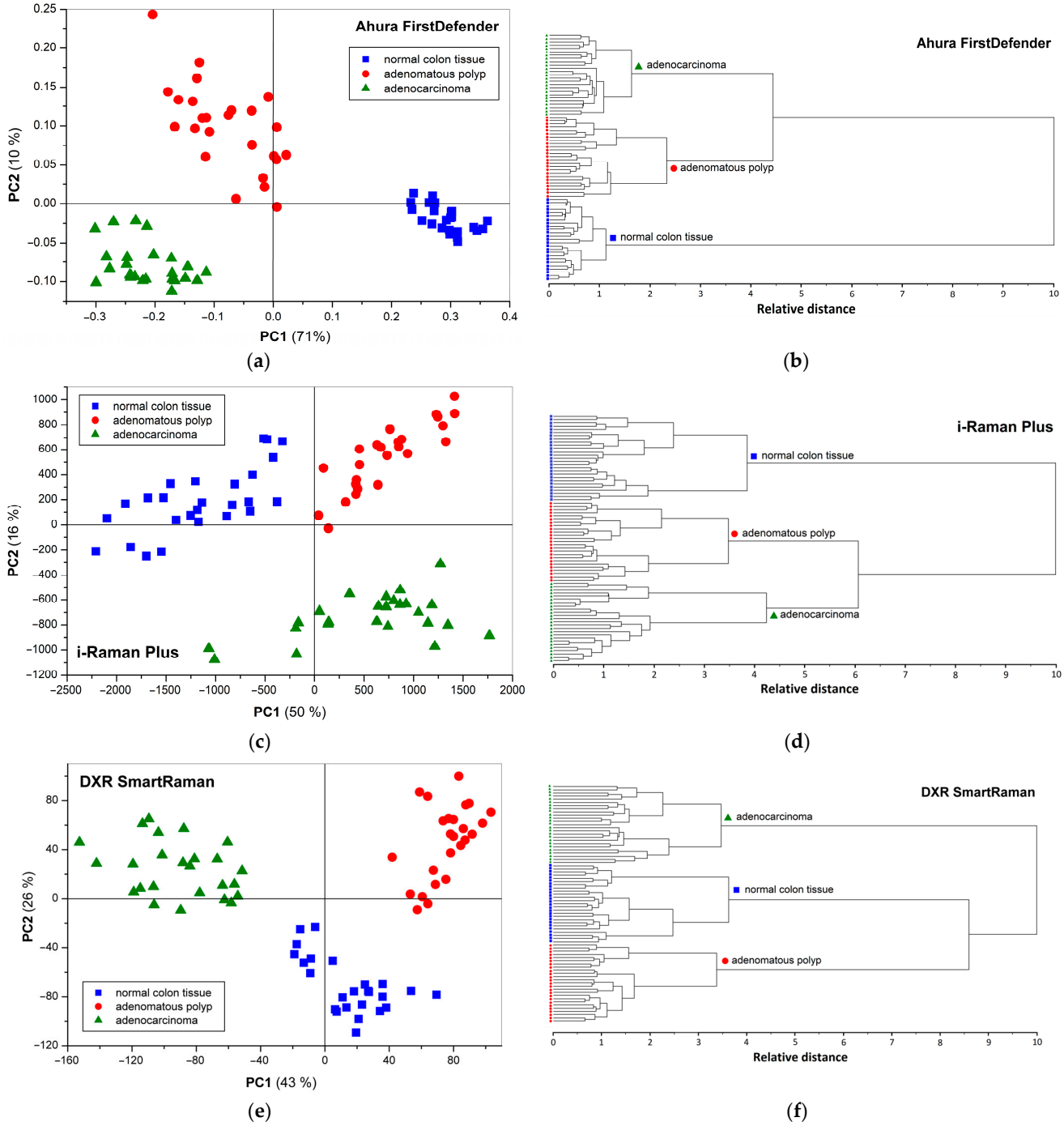

Figure 6. Discrimination of the samples of normal colon tissue (blue squares), adenomatous polyp (red circles), and adenocarcinoma (green triangles) based on the PCA and HCA of individual Raman spectra recorded using handheld (**a**,**b**), modular (**c**,**d**), and laboratory (**e**,**f**) Raman instruments at the 25–30 independent sites of samples: (left panels) component score plots of PC1 versus PC2; (right panels) dendrograms of similarity obtained via HCA using Ward's clustering method and squared Euclidean distances.

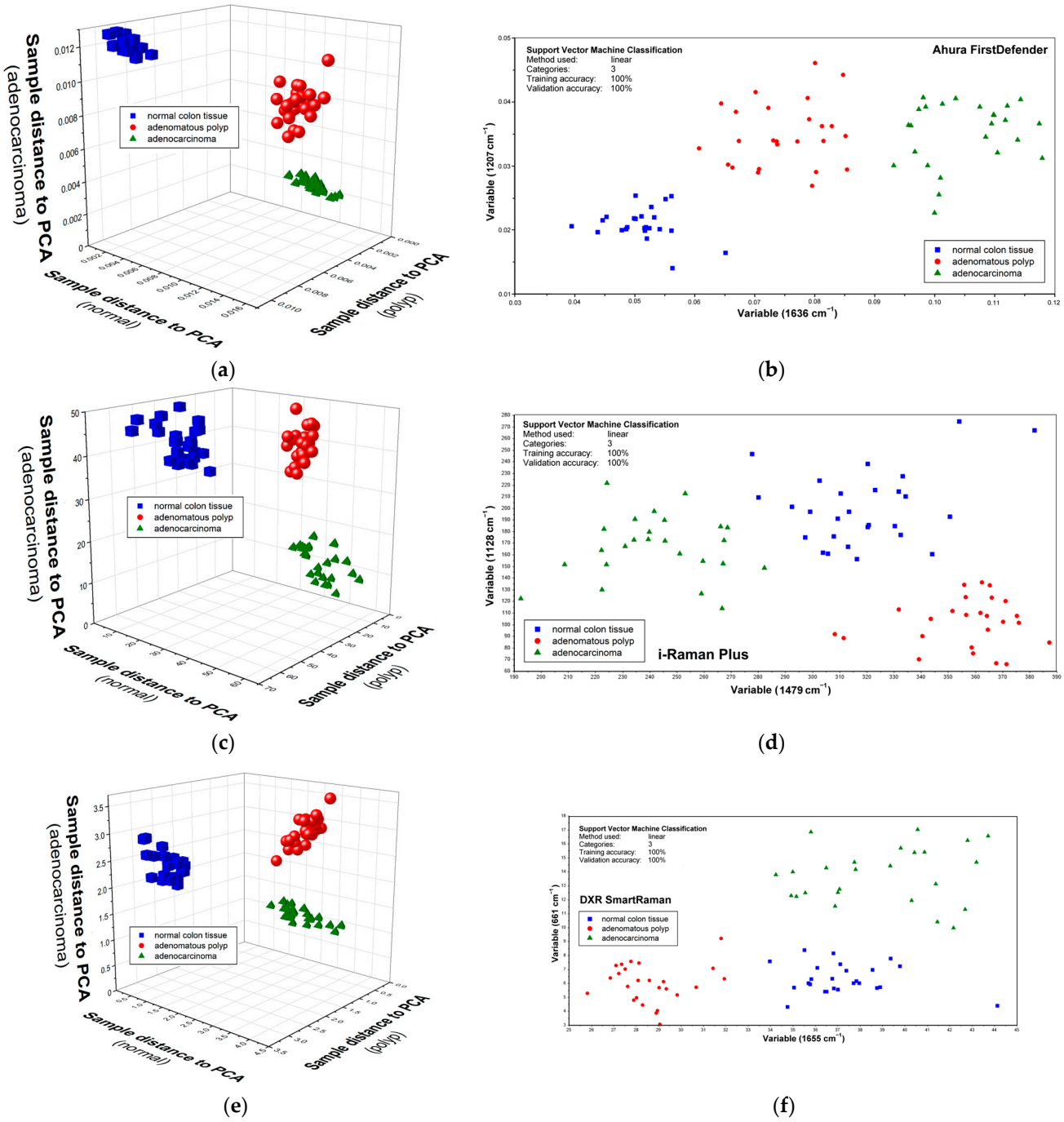

Figure 7. Classification of the samples of normal colon tissue (blue squares), adenomatous polyp (red circles), and adenocarcinoma (green triangles) based on the analyses of individual Raman data recorded with handheld (**a**,**b**), modular (**c**,**d**), and laboratory (**e**,**f**) Raman instruments at the 25–30 independent sites of samples: (left panels) 3D Cooman's plots for the SIMCA classification; (right panels) scattergram based on SVM classification.

SVM is an effective tool for classifying spectral data due to the following advantages [54,66]: (a) it produces a robust classifier that can work with small or limited-size datasets; (b) it uses a structural risk minimization (SRM) approach, which reduces the risk of overfitting the data; (c) it gives reproducible solutions when using the same classifier parameters; (d) it can draw class boundaries with complex conditions, replacing kernel functions. Three Raman datasets obtained from the laboratory, modular, and portable devices, which include 25 spectra for each group, were used as training datasets to perform

SVM classification training to fully distinguish the three types of samples, i.e., normal colon tissue, adenomatous polyp, and adenocarcinoma. The scattergrams, characterizing the three Raman instruments, are shown in Figure 7b,d,f. All the obtained SVM classifications allowed us to distinguish between the three mentioned types of colon tissue.

4. Conclusions

The results of this study suggest that portable Raman spectrometers, both handheld and modular, equipped with an excitation source at 785 nm possess satisfactory Raman spectra of colon tissues and reference biopolymer compounds. The spectra measured using Ahura FirstDefender and i-Raman Plus have intense and well-resolved bands. Important spectral parameters, such as the ratio of the principal signals to the noise level or the half-width of these signals, were determined and found to be suitable for all instruments tested. For these devices, the prominent intense Raman bands of colon tissue biochemical markers occurred at the correct wavenumber positions comparable to previously published values and the values obtained using the laboratory instrument. The DXR SmartRaman spectrometer detected even small changes in the signal intensity or position for adenomatous polyp and adenocarcinoma samples, which could be critical for early diagnosis. In contrast, for the handheld device and, to a lesser extent, the modular one, the band overlap did not permit the detection of some of these spectral features.

Laboratory and portable Raman instruments were used successfully to discriminate and classify normal, benign, and malignant colon tissues using appropriate multivariate statistical methods. Despite its less pronounced spectral characteristics, the handheld Raman spectrometer can be used in early diagnosis of colorectal carcinoma, comparable to the modular and laboratory instruments. In addition, its ease of use, small size, and rapid measurement of biological samples make it an attractive tool for medical practice.

Supplementary Materials: The following supporting information can be downloaded at: https://www.mdpi.com/article/10.3390/app14020791/s1, Figure S1: Peak decomposition of the Raman spectra of calf thymus DNA obtained with laboratory, modular, and handheld instruments. Table S1. Raman band assignments for the reference compounds. Table S2. Contribution of biological macromolecules in the Raman spectra of normal colon tissue.

Author Contributions: Conceptualization, A.S. and L.P.; methodology, A.S. and J.P.; software, A.S.; validation, A.S., D.J. and M.V.; formal analysis, A.S., Z.K., D.J. and M.V.; investigation, A.S. and J.P.; resources, M.V. and J.P.; data curation, A.S.; writing—original draft preparation, A.S.; writing—review and editing, A.S.; visualization, A.S. and D.J.; supervision, A.S.; project administration, L.P.; funding acquisition, L.P. All authors have read and agreed to the published version of the manuscript.

Funding: This research was funded by the Ministry of Health of the Czech Republic; grant number NU20-09-00229.

Institutional Review Board Statement: The study was conducted according to the guidelines of the Declaration of Helsinki and approved by the Ethics Committee of the First Faculty of Medicine and the General University Hospital in Prague (Project NU20-09-00229, 18 June 2020).

Informed Consent Statement: Informed consent was obtained from all subjects involved in the study.

Data Availability Statement: Data are contained within the article.

Conflicts of Interest: The authors declare no conflict of interest. The funders had no role in the design of the study; in the collection, analyses, or interpretation of data; in the writing of the manuscript; or in the decision to publish the results.

References

1. Taheri, H.; Gonzalez Bocanegra, M.; Taheri, M. Artificial Intelligence, Machine Learning and Smart Technologies for Nondestructive Evaluation. *Sensors* **2022**, *22*, 4055. [CrossRef] [PubMed]
2. Maida, M.; Macaluso, F.S.; Ianiro, G.; Mangiola, F.; Sinagra, E.; Hold, G.; Maida, C.; Cammarota, G.; Gasbarrini, A.; Scarpulla, G. Screening of colorectal cancer: Present and future. *Expert Rev. Anticancer. Ther.* **2017**, *17*, 1131–1146. [CrossRef] [PubMed]

3. Upchurch, E.; Isabelle, M.; Lloyd, G.R.; Kendall, C.; Barr, H. An update on the use of Raman spectroscopy in molecular cancer diagnostics: Current challenges and further prospects. *Expert Rev. Mol. Diagn.* **2018**, *18*, 245–258. [CrossRef] [PubMed]
4. Smith, E.; Dent, G. *Modern Raman Spectroscopy: A Practical Approach*, 2nd ed.; John Wiley & Sons: New York, NY, USA, 2019; pp. 1–256.
5. Talari, A.C.S.; Movasaghi, Z.; Rehman, S.; Rehman, I.U. Raman spectroscopy of biological tissues. *Appl. Spectrosc. Rev.* **2015**, *50*, 46–111. [CrossRef]
6. Beljebbar, A.; Bouché, O.; Diébold, M.D.; Guillou, P.J.; Palot, J.P.; Eudes, D.; Manfait, M. Identification of Raman spectroscopic markers for the characterization of normal and adenocarcinomatous colonic tissues. *Crit. Rev. Oncol. Hematol.* **2009**, *72*, 255–264. [CrossRef] [PubMed]
7. Pence, I.; Mahadevan-Jansen, A. Clinical instrumentation and applications of Raman spectroscopy. *Chem. Soc. Rev.* **2016**, *45*, 1958–1979. [CrossRef]
8. Kourkoumelis, N.; Balatsoukas, I.; Moulia, V.; Elka, A.; Gaitanis, G.; Bassukas, I.D. Advances in the in vivo Raman spectroscopy of malignant skin tumors using portable instrumentation. *Int. J. Mol. Sci.* **2015**, *16*, 14554–14570. [CrossRef]
9. Avram, L.; Iancu, S.D.; Stefancu, A.; Moisoiu, V.; Colnita, A.; Marconi, D.; Donca, V.; Buzdugan, E.; Craciun, R.; Leopold, N.; et al. SERS-based liquid biopsy of gastrointestinal tumors using a portable Raman device operating in a clinical environment. *J. Clin. Med.* **2020**, *9*, 212. [CrossRef]
10. Tripathy, S.; Chavva, S.; Coté, G.L.; Mabbott, S. Modular and Handheld Raman Systems for SERS-based point-of-care diagnostics. *Curr. Opin. Biomed. Eng.* **2023**, *28*, 100488. [CrossRef]
11. Kranenburg, R.F.; Verduin, J.; de Ridder, R.; Weesepoel, Y.; Alewijn, M.; Heerschop, M.; Keizers, P.H.; van Esch, A.; van Asten, A.C. Performance evaluation of handheld Raman spectroscopy for cocaine detection in forensic case samples. *Drug Testing Anal.* **2021**, *13*, 1054–1067. [CrossRef]
12. Deidda, R.; Sacre, P.Y.; Clavaud, M.; Coïc, L.; Avohou, H.; Hubert, P.; Ziemons, E. Vibrational spectroscopy in analysis of pharmaceuticals: Critical review of innovative portable and handheld NIR and Raman spectrophotometers. *TrAC Trends Anal. Chem.* **2019**, *114*, 251–259. [CrossRef]
13. Mosca, S.; Lin, Q.; Stokes, R.; Bharucha, T.; Gangadharan, B.; Clarke, R.; Fernandez, L.G.; Deats, M.; Walsby-Tickle, J.; Arman, B.Y.; et al. Innovative method for rapid detection of falsified COVID-19 vaccines through unopened vials using handheld Spatially Offset Raman Spectroscopy (SORS). *Vaccine* **2023**, *41*, 6960–6968. [CrossRef] [PubMed]
14. Li Vigni, M.; Durante, C.; Michelini, S.; Nocetti, M.; Cocchi, M. Preliminary assessment of Parmigiano Reggiano authenticity by handheld Raman spectroscopy. *Foods* **2020**, *9*, 1563. [CrossRef] [PubMed]
15. Müller-Maatsch, J.; van Ruth, S.M. Handheld devices for food authentication and their applications: A review. *Foods* **2021**, *10*, 2901. [CrossRef] [PubMed]
16. Gonzalez-Gonzalez, C.R.; Hansen, M.; Stratakos, A.C. Rapid Identification of Foodborne Pathogens in Limited Resources Settings Using a Handheld Raman Spectroscopy Device. *Appl. Sci.* **2022**, *12*, 9909. [CrossRef]
17. Sato, S.; Sekine, R.; Kagoshima, H.; Kazama, K.; Kato, A.; Shiozawa, M.; Tanaka, J.I. All-in-one Raman spectroscopy approach to diagnosis of colorectal cancer: Analysis of spectra in the fingerprint regions. *J. Anus Rectum Colon* **2019**, *3*, 84–90. [CrossRef]
18. Sekine, R.; Sato, S.; Tanaka, J.I.; Kagoshima, H.; Aoki, T.; Murakami, M. Potential Application of Raman Spectroscopy for Real-time Diagnosis and Classification of Colorectal Cancer. *Showa Univ. J. Med. Sci.* **2018**, *30*, 381–389. [CrossRef]
19. Sato, S.; Kagoshima, H.; Shiozawa, M.; Nukada, S.; Iguchi, K.; Mikayama, Y.; Oshima, T.; Numata, M.; Tamagawa, H.; Rino, Y.; et al. Automated non-invasive identification of pelvic autonomic nerves with a handheld Raman spectrometer and potential application to nerve-sparing colorectal surgery: A preliminary study in surgical specimens. *Transl. Cancer Res.* **2021**, *10*, 3921. [CrossRef]
20. Xie, Y.H.; Chen, Y.X.; Fang, J.Y. Comprehensive review of targeted therapy for colorectal cancer. *Signal Transduct. Target. Ther.* **2020**, *5*, 22. [CrossRef]
21. Schreuders, E.H.; Ruco, A.; Rabeneck, L.; Schoen, R.E.; Sung, J.J.; Young, G.P.; Kuipers, E.J. Colorectal cancer screening: A global overview of existing programmes. *Gut* **2015**, *64*, 1637–1649. [CrossRef]
22. Kanth, P.; Inadomi, J.M. Screening and prevention of colorectal cancer. *BMJ* **2021**, *374*, n1855. [CrossRef] [PubMed]
23. Zessner-Spitzenberg, J.; Jiricka, L.; Waldmann, E.; Rockenbauer, L.-M.; Cook, J.; Hinterberger, A.; Majcher, B.; Szymanska, A.; Asaturi, A.; Trauner, M.; et al. Polyp characteristics at screening colonoscopy and post-colonoscopy colorectal cancer mortality: A retrospective cohort study. *Gastrointest. Endosc.* **2023**, *97*, 1109. [CrossRef] [PubMed]
24. Zessner-Spitzenberg, J.; Waldmann, E.; Jiricka, L.; Rockenbauer, L.-M.; Hinterberger, A.; Cook, J.; Asaturi, A.; Szymanska, A.; Majcher, B.; Trauner, M.; et al. Comparison of adenoma detection rate and proximal serrated polyp detection rate and their effect on post-colonoscopy colorectal cancer mortality in screening patients. *Endoscopy* **2023**, *55*, 434–441. [CrossRef] [PubMed]
25. Lin, D.H.M.; Manara, D.; Lindqvist-Reis, P.; Fanghänel, T.; Mayer, K. The use of different dispersive Raman spectrometers for the analysis of uranium compounds. *Vib. Spectrosc.* **2014**, *73*, 102–110.
26. Jehlička, J.; Culka, A. Critical evaluation of portable Raman spectrometers: From rock outcrops and planetary analogs to cultural heritage–A review. *Anal. Chim. Acta* **2022**, *1209*, 339027. [CrossRef] [PubMed]
27. Košek, F.; Culka, A.; Rousaki, A.; Vandenabeele, P.; Jehlička, J. Evaluation of handheld and portable Raman spectrometers with different laser excitation wavelengths for the detection and characterization of organic minerals. *Spectrochim. Acta A Mol. Biomol. Spectrosc.* **2020**, *243*, 118818. [CrossRef] [PubMed]

28. Culka, A.; Jehlička, J.; Edwards, H.G.M. Acquisition of Raman spectra of amino acids using portable instruments: Outdoor measurements and comparison. *Spectrochim. Acta Part A Mol. Biomol. Spectrosc.* **2010**, *77*, 978–983. [CrossRef]
29. Safar, W.; Azziz, A.; Edely, M.; Lamy de la Chapelle, M. Conventional Raman, SERS and TERS Studies of DNA Compounds. *Chemosensors* **2023**, *11*, 399. [CrossRef]
30. Sofińska, K.; Wilkosz, N.; Szymoński, M.; Lipiec, E. Molecular spectroscopic markers of DNA damage. *Molecules* **2020**, *25*, 561. [CrossRef]
31. Benevides, J.M.; Overman, S.A.; Thomas Jr, G.J. Raman, polarized Raman and ultraviolet resonance Raman spectroscopy of nucleic acids and their complexes. *J. Raman Spectrosc.* **2005**, *36*, 279–299. [CrossRef]
32. Rygula, A.; Majzner, K.; Marzec, K.M.; Kaczor, A.; Pilarczyk, M.; Baranska, M. Raman spectroscopy of proteins: A review. *J. Raman Spectrosc.* **2013**, *44*, 1061–1076. [CrossRef]
33. Kuhar, N.; Sil, S.; Umapathy, S. Potential of Raman spectroscopic techniques to study proteins. *Spectrochim. Acta A Mol. Biomol. Spectrosc.* **2021**, *258*, 119712. [CrossRef]
34. Sjöberg, B.; Foley, S.; Cardey, B.; Enescu, M. An experimental and theoretical study of the amino acid side chain Raman bands in proteins. *Spectrochim. Acta A Mol. Biomol. Spectrosc.* **2014**, *128*, 300–311. [CrossRef] [PubMed]
35. Naomi, R.; Ridzuan, P.M.; Bahari, H. Current insights into collagen type I. *Polymers* **2021**, *13*, 2642. [CrossRef] [PubMed]
36. Martinez, M.G.; Bullock, A.J.; MacNeil, S.; Rehman, I.U. Characterisation of structural changes in collagen with Raman spectroscopy. *Appl. Spectrosc. Rev.* **2019**, *54*, 509–542. [CrossRef]
37. Synytsya, A.; Janstová, D.; Šmidová, M.; Synytsya, A.; Petrtýl, J. Evaluation of IR and Raman spectroscopic markers of human collagens: Insides for indicating colorectal carcinogenesis. *Spectrochim. Acta A Mol. Biomol. Spectrosc.* **2023**, *296*, 122664. [CrossRef]
38. Cárcamo-Vega, J.J.; Brañes, M.R.; Loske, A.M.; Campos-Vallette, M.M. The influence of the number of shock waves and the energy flux density on the Raman spectrum of collagen type I from rat. *Shock. Waves* **2020**, *30*, 201–214. [CrossRef]
39. Fallacara, A.; Baldini, E.; Manfredini, S.; Vertuani, S. Hyaluronic acid in the third millennium. *Polymers* **2018**, *10*, 701. [CrossRef]
40. Ucm, R.; Aem, M.; Lhb, Z.; Kumar, V.; Taherzadeh, M.J.; Garlapati, V.K.; Chandel, A.K. Comprehensive review on biotechnological production of hyaluronic acid: Status, innovation, market and applications. *Bioengineered* **2022**, *13*, 9645–9661. [CrossRef]
41. La Verde, G.; Sasso, A.; Rusciano, G.; Capaccio, A.; Fusco, S.; Mayol, L.; Biondi, M.; Silvestri, T.; Netti, P.A.; La Commara, M.; et al. Characterization of Hyaluronic Acid-Coated PLGA Nanoparticles by Surface-Enhanced Raman Spectroscopy. *Int. J. Mol. Sci.* **2023**, *24*, 601. [CrossRef]
42. Ellis, R.; Green, E.; Winlove, C.P. Structural analysis of glycosaminoglycans and proteoglycans by means of Raman microspectrometry. *Connect. Tissue Res.* **2009**, *50*, 29–36. [CrossRef] [PubMed]
43. Andrade, P.O.; Bitar, R.A.; Yassoyama, K.; Martinho, H.; Santo, A.M.E.; Bruno, P.M.; Martin, A.A. Study of normal colorectal tissue by FT-Raman spectroscopy. *Anal. Bioanal. Chem.* **2007**, *387*, 1643–1648. [CrossRef]
44. Synytsya, A.; Judexova, M.; Hoskovec, D.; Miskovicova, M.; Petruzelka, L. Raman spectroscopy at different excitation wavelengths (1064, 785 and 532 nm) as a tool for diagnosis of colon cancer. *J. Raman Spectrosc.* **2014**, *45*, 903–911. [CrossRef]
45. Synytsya, A.; Vaňková, A.; Miškovičová, M.; Petrtýl, J.; Petruželka, L. Ex Vivo Vibration Spectroscopic Analysis of Colorectal Polyps for the Early Diagnosis of Colorectal Carcinoma. *Diagnostics* **2021**, *11*, 2048. [CrossRef]
46. Fousková, M.; Vališ, J.; Synytsya, A.; Habartová, L.; Petrtýl, J.; Petruželka, L.; Setnička, V. In vivo Raman spectroscopy in the diagnostics of colon cancer. *Analyst* **2023**, *148*, 2518–2526. [CrossRef] [PubMed]
47. Brozek-Pluska, B.; Musial, J.; Kordek, R.; Abramczyk, H. Analysis of human colon by Raman spectroscopy and imaging-elucidation of biochemical changes in carcinogenesis. *Int. J. Mol. Sci.* **2019**, *20*, 3398. [CrossRef] [PubMed]
48. Wiercigroch, E.; Szafraniec, E.; Czamara, K.; Pacia, M.Z.; Majzner, K.; Kochan, K.; Kaczor, A.; Baranska, M.; Malek, K. Raman and infrared spectroscopy of carbohydrates: A review. *Spectrochim. Acta A Mol. Biomol. Spectrosc.* **2017**, *185*, 317–335. [CrossRef]
49. Czamara, K.; Majzner, K.; Pacia, M.Z.; Kochan, K.; Kaczor, A.; Baranska, M. Raman spectroscopy of lipids: A review. *J. Raman Spectrosc.* **2015**, *46*, 4–20. [CrossRef]
50. Brozek-Pluska, B.; Miazek, K.; Musiał, J.; Kordek, R. Label-free diagnostics and cancer surgery Raman spectra guidance for the human colon at different excitation wavelengths. *RSC Adv.* **2019**, *9*, 40445–40454. [CrossRef]
51. Liu, W.; Sun, Z.; Chen, J.; Jing, C. Raman spectroscopy in colorectal cancer diagnostics: Comparison of PCA-LDA and PLS-DA models. *J. Spectrosc.* **2016**, *2016*, 1603609. [CrossRef]
52. Bergholt, M.S.; Zheng, W.; Lin, K.; Wang, J.; Xu, H.; Ren, J.L.; Ho, K.Y.; The, M.; Yeoh, K.G.; Huang, Z. Characterizing variability of in vivo Raman spectroscopic properties of different anatomical sites of normal colorectal tissue towards cancer diagnosis at colonoscopy. *Anal. Chem.* **2015**, *87*, 960–966. [CrossRef]
53. de Carvalho, L.F.D.C.E.S.; Bitar, R.A.; Arisawa, E.Â.L.; Brandão, A.A.H.; Honorio, K.M.; Cabral, L.A.G.; Martin, A.A.; Martinho, H.D.S.; Almeida, J.D. Spectral region optimization for Raman-based optical biopsy of inflammatory lesions. *Photomed. Laser Surg.* **2010**, *28*, S-111. [CrossRef] [PubMed]
54. Widjaja, E.; Zheng, W.; Huang, Z. Classification of colonic tissues using near-infrared Raman spectroscopy and support vector machines. *Int. J. Oncol.* **2008**, *32*, 653–662. [CrossRef] [PubMed]
55. Molckovsky, A.; Song, L.M.W.K.; Shim, M.G.; Marcon, N.E.; Wilson, B.C. Diagnostic potential of near-infrared Raman spectroscopy in the colon: Differentiating adenomatous from hyperplastic polyps. *Gastrointestin. Endosc.* **2003**, *57*, 396–402. [CrossRef] [PubMed]
56. Chowdary, M.V.P.; Kumar, K.K.; Thakur, K.; Anand, A.; Kurien, J.; Krishna, C.M.; Mathew, S. Discrimination of normal and malignant mucosal tissues of the colon by Raman spectroscopy. *Photomed. Laser Surg.* **2007**, *25*, 269–274. [CrossRef] [PubMed]

57. Vogler, N.; Bocklitz, T.; Subhi Salah, F.; Schmidt, C.; Bräuer, R.; Cui, T.; Mireskandari, M.; Greten, F.R.; Schmitt, M.; Stallmach, A.; et al. Systematic evaluation of the biological variance within the Raman based colorectal tissue diagnostics. *J. Biophotonics* **2016**, *9*, 533–541. [CrossRef] [PubMed]
58. Wu, X.; Li, S.; Xu, Q.; Yan, X.; Fu, Q.; Fu, X.; Fang, X.; Zhang, Y. Rapid and accurate identification of colon cancer by Raman spectroscopy coupled with convolutional neural networks. *Jpn. J. Appl. Phys.* **2021**, *60*, 067001. [CrossRef]
59. Kalatzis, D.; Spyratou, E.; Karnachoriti, M.; Kouri, M.A.; Orfanoudakis, S.; Koufopoulos, N.; Pouliakis, A.; Danias, N.; Seimenis, I.; Kontos, A.G.; et al. Advanced Raman Spectroscopy Based on Transfer Learning by Using a Convolutional Neural Network for Personalized Colorectal Cancer Diagnosis. *Optics* **2023**, *4*, 310–320. [CrossRef]
60. Cao, Z.; Pan, X.; Yu, H.; Hua, S.; Wang, D.; Chen, D.Z.; Zhou, M.; Wu, J. A deep learning approach for detecting colorectal cancer via Raman spectra. *BME Front.* **2022**, *2022*, 9872028. [CrossRef]
61. Blake, N.; Gaifulina, R.; Griffin, L.D.; Bell, I.M.; Rodriguez-Justo, M.; Thomas, G.M. Deep Learning Applied to Raman Spectroscopy for the Detection of Microsatellite Instability/MMR Deficient Colorectal Cancer. *Cancers* **2023**, *15*, 1720. [CrossRef]
62. Kuzmin, A.N.; Pliss, A.; Rzhevskii, A.; Lita, A.; Larion, M. BCAbox algorithm expands capabilities of Raman microscope for single organelles assessment. *Biosensors* **2018**, *8*, 106. [CrossRef]
63. Geyik, G.A.; Cengiz, B.P.; Tugrul, F.; Elmas, S.N.K.; Yilmaz, I.; Arslan, F.N. A rapid diagnostic approach for gastric and colon cancers via Fourier transform mid–infrared spectroscopy coupled with chemometrics from paraffin–embedded tissues. *Spectrochim. Acta A Mol. Biomol. Spectrosc.* **2022**, *267*, 120619.
64. Tugrul, F.; Geyik, G.A.; Kaya, B.Y.; Cengiz, B.P.; Elmas, S.N.K.; Yilmaz, I.; Arslan, F.N. A biospectroscopic approach toward colorectal cancer diagnosis from bodily fluid samples via ATR–MIR spectroscopy combined with multivariate data analysis. *Spectrochim. Acta A Mol. Biomol. Spectrosc.* **2024**, *304*, 123342. [CrossRef] [PubMed]
65. Khanmohammadi, M.; Garmarudi, A.B.; Ghasemi, K.; Jaliseh, H.K.; Kaviani, A. Diagnosis of colon cancer by attenuated total reflectance-fourier transform infrared microspectroscopy and soft independent modeling of class analogy. *Med. Oncol.* **2009**, *26*, 292–297. [CrossRef]
66. Fu, J.J.; Yu, Y.W.; Lin, H.M.; Chai, J.W.; Chen, C.C.C. Feature extraction and pattern classification of colorectal polyps in colonoscopic imaging. *Comput. Med. Imaging Graph.* **2014**, *38*, 267–275. [CrossRef]